Title
Multiple colliding laser pulses as a basis for studying high-field high-energy physics

Journal
Physical Review A, 100(6)

ISSN
2469-9926

Authors
Magnusson, J
Gonoskov, A
Marklund, M
et al.

Publication Date
2019-12-01

DOI
10.1103/physreva.100.063404

Peer reviewed

Multiple colliding laser pulses as a basis for studying high-field high-energy physics

J. Magnusson,[1,*] A. Gonoskov,[2,3,4] M. Marklund,[2] T. Zh. Esirkepov,[5] J. K. Koga,[5] K. Kondo,[5] M. Kando,[5] S. V. Bulanov,[5,6,7] G. Korn,[6] C. G. R. Geddes,[8] C. B. Schroeder,[8] E. Esarey,[8] and S. S. Bulanov[8]

[1]*Department of Physics, Chalmers University of Technology, 41296 Gothenburg, Sweden*
[2]*Department of Physics, University of Gothenburg, 41296 Gothenburg, Sweden*
[3]*Institute of Applied Physics, Russian Academy of Sciences, Nizhny Novgorod 603950, Russia*
[4]*Lobachevsky State University of Nizhni Novgorod, Nizhny Novgorod 603950, Russia*
[5]*Kansai Photon Science Institute, National Institutes for Quantum and Radiological Science and Technology, 8-1-7 Umemidai, Kizugawa, Kyoto 619-0215, Japan*
[6]*Institute of Physics ASCR, ELI-Beamlines Project, 182 21 Prague, Czech Republic*
[7]*Prokhorov General Physics Institute, Russian Academy of Sciences, Vavilov Street 38, Moscow 119991, Russia*
[8]*Lawrence Berkeley National Laboratory, Berkeley, California 94720, USA*

Apart from maximizing the strength of optical electromagnetic fields achievable at high-intensity laser facilities, the collision of several phase-matched laser pulses has been identified theoretically as a trigger of and way to study various phenomena. These range from the basic processes of strong-field quantum electrodynamics to the extraordinary dynamics of the generated electron-positron plasmas. This has paved the way for several experimental proposals aimed at both fundamental studies of matter at extreme conditions and the creation of particle and radiation sources. Because of the unprecedented capabilities of such sources, they have the potential to open up new opportunities for experimental studies in nuclear and quark-gluon physics. We perform here a systematic analysis of different regimes and opportunities achievable with the concept of multiple colliding laser pulses, for both current and upcoming laser facilities. We reveal that several distinct regimes could be within reach of multi-petawatt laser facilities.

I. INTRODUCTION

Studies of the interaction between charged particles with electromagnetic (EM) fields of high intensity have revealed a large number of phenomena and have received increasing attention over the past decade [1–3]. This attention is not only due to the diversity of phenomena enabled by strong fields, but also because of the emerging experimental capabilities that, apart from collider-type experiments [4–7], will provide opportunities for performing experiments in many other configurations. The next generation of laser facilities, such as ELI Beamlines, ELI NP, CoReLS, Apollon, XCELS, and Vulcan 10 PW [8–13], as well as future lepton colliders [14] are expected to operate in a regime where these phenomena either dominate or significantly influence the interaction.

According to quantum electrodynamics (QED), the action of strong EM fields can lead to the photon emission of an electron (Compton process [15–17]), the photon decay into electron-positron pairs (Breit-Wheeler process [16,18,19]), and the electron-positron pair production from vacuum (Schwinger process [20–22]). In forthcoming experiments the field intensity can be so high that the two former processes appear in rapid succession, leading to a cascaded production of electrons, positrons, and high-energy photons [23–25]. Apart from the shower-type cascade, which implies a repeated division of the energy of the initial particle or photon, high-intensity lasers also open up the possibility for running avalanche-type cascades, in which the electromagnetic fields both accelerate particles and cause the QED processes [24,26]. Such a cascade can be initiated by the seed particles of energetic particle beams, a background plasma, or even the Schwinger process. These cascades are fascinating phenomena of rapid transformation of laser and charged particle beam energy into high-energy photons and electron-positron pairs.

In order to trigger these processes one needs to reach a certain strength of the electromagnetic field. This raises the problem of finding the optimal strategy of focusing laser radiation. One such strategy, first found to be advantageous for enhancing the electron-positron pair production, is the concept of multiple colliding laser pulses (MCLPs) [27]. In this concept, a laser beam is split into N equal subbeams that are subsequently combined constructively at the focus. The energy of the unsplit laser beam $\mathcal{E}_1$ is related to its peak electric field E_1 and peak intensity I_1 as $\mathcal{E}_1 \sim E_1^2 \sim I_1$. Each subbeam receives an energy of $\mathcal{E}_1/N$ and, with identical focusing, has a peak electric field of $E_1/\sqrt{N}$ and intensity of I_1/N. A constructive interference of the subbeams therefore gives an electric field of $E_N = \sqrt{N}E_1$ and an intensity of $I_N = NI_1$, which can be significantly higher than for a single unsplit beam. However, for a large number of subbeams the peak value of the electric field at focus E_N is obviously constrained by the diffraction limit. The problem of maximizing the field strength is limited by the optimal case, which can be viewed

*joel.magnusson@chalmers.se

as the inverse emission of a dipole antenna. Therefore, the resulting field structure is often also referred to as a dipole wave and represents an accessible form for theoretical analysis [25,28,29].

For monochromatic fields, the dipole wave has been shown to provide the highest possible field strength $a_0 \approx 780\sqrt{P/1\ \mathrm{PW}}$ for a given power P [30] and it has also been shown that this field configuration is beneficial for the generation of QED cascades [31–33] (the field strength is hereafter written in relativistic units that will be rigorously defined later). Apart from enhancing pair production due to the Breit-Wheeler process, the dipole wave also has the interesting property of trapping charged particles near the maxima of its electric field, for sufficiently high field intensities [34]. This is referred to as *anomalous* radiative trapping in order to differentiate from the normal radiative trapping that occurs at the magnetic- (electric-) field maxima (minima) due to gyration of electrons that rapidly exhaust their energy through radiation losses [35]. It is noteworthy, however, that anomalous radiative trapping not only occurs in dipole waves, but is a more universal feature that originates from the general tendency of charged particles to align their motion along the radiation-free direction [36] when they rapidly lose energy and enter the radiation-dominated regime [25,37]. This can even be observed in simple mechanical systems with strong friction forces [38]. It has also been recently shown that charged particles in the strong EM fields formed by two colliding pulses tend to move along trajectories that are defined by either attractors or limit cycles [35,39–42]. This analysis was later expanded to the case of MCLPs, for which similar phase-space patterns could be observed [43]. While such behavior is mostly attributed to intense radiation losses that are typically modeled based on the classical description of radiation reaction, in terms of either a Landau-Lifshitz (LL) equation of motion or a "modified" LL equation [43,44], the mechanisms behind the observed phenomena are tolerant to the quantized nature of emission and similar behavior has also been observed in computer simulations based on probabilistic quantum treatment of radiation losses [34,36,39,40].

A more complete treatment based on simulations that also account for pair production and therefore QED cascades [45–51] has helped reveal a fortunate interplay between the cascade and anomalous radiative trapping in the focus of a dipole wave. The trapping mechanism causes a migration of particles to the focus where the strong field makes them gain energy and emit high-energy photons that in turn have a high chance of decaying into a pair of particles. Even if the original particle leaves the system due to insufficient radiation losses, the generated particles of lower energy might be trapped, replenishing the overall number of particles undergoing the trapped motion. This leads to the triggering of self-sustained locally confined QED cascades for laser powers as low as $P = 7.2$ PW [33], which is drastically lower than the 60 PW required for a prominent appearance of anomalous radiative trapping in single-particle dynamics [34]. For $P \gtrsim 8$ PW the exponential growth of the number of particles in such a trapped QED cascade makes it possible to reach extreme states of electron-positron plasma in terms of both a high density and high energy of particles and photons. Moreover, the self-action of the tremendous current produced by counterpropagating electrons and positrons in the oscillating dipole field leads to the growth of an instability followed by a collapse into ultrathin radial sheets [52] and, for $P > 20$ PW, into an axial pinch [53].

The trapping of charged particles at the maxima of strong EM fields should result in an enhanced emission of high-energy photons. Indeed, it has been shown that in the interaction of a dipole wave with an underdense plasma, a fraction of the plasma electrons get trapped at the focus and oscillate along the symmetry axis of the wave, producing a bidirectional source of GeV photons [33]. However, the maximum quiver energy of an electron in this field is $\gamma \sim 2a_0$, which implies a maximum photon energy of $\hbar\omega \sim 0.8\sqrt{P/1\ \mathrm{PW}}$ GeV. This limits the energy of the emitted photons to a few GeV for upcoming 10-PW facilities. In order to produce photon energies beyond this limit, in the tens of GeV, the interaction of a highly energetic electron beam with a dipole wave was suggested in Ref. [54]. In this configuration it is interesting to note that, above a certain threshold, increasing the laser power will not lead to a more efficient generation of high-energy photons. It will instead drive an increasingly stronger shower cascade, hampering the yield of high-energy photons. In fact, this was shown to also be the case for more general field structures and, while allowing for a higher efficiency, is therefore not exclusive to the dipole wave. For the purpose of efficiently generating photons above a few GeV it was found that there is an optimal laser power of $P \approx 0.4$ PW for a dipole wave, around which ~20% of the initial electrons can be converted into high-energy photons.[1] Altogether, these results show the flexibility of the MCLP configuration and thereby the possibility of studying several distinct regimes of interaction, depending primarily on values of laser power and electron-beam energy.

In this paper we study the interaction of an electron beam with MCLPs, where the beam is directed along the symmetry axis of the MCLP configuration. This allows the electrons to reach the highest EM-field strengths without a significant loss of energy or lateral scattering. The electron beam can therefore remain well collimated until it reaches the focus of the MCLP configuration (see Fig. 1), maximizing the chance of trapping electrons in the EM field as they are exposed to the highest intensity. It also opens up a possibility to study the interaction of charged particle with supercritical fields, which is currently an active topic of discussion [55–58]. As mentioned, this setup is also advantageous for high-energy photon production for certain values of laser power. We here identify several areas in the electron-beam-energy laser-power parameter space, favoring the development of shower- or avalanche-type cascades, high-energy photon production, or electron-beam-energy depletion. Thus, the proposed configuration may also provide a solution for effectively stopping high-energy electron beams over micrometer-scale distances.

The paper is organized as follows. Section II provides a brief overview of the analytical form of the dipole wave

[1] We define here high-energy photons as those carrying an energy equal to or larger than half the initial electron energy.

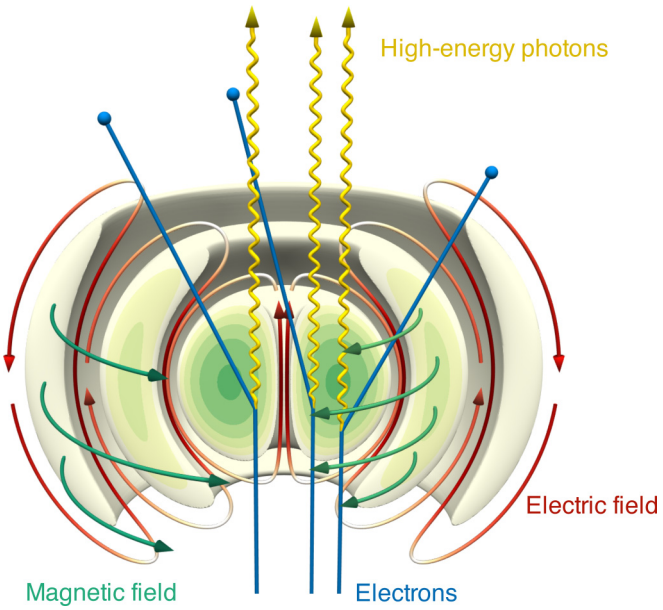

FIG. 1. Conceptual visualization of the setup, where high-energy electrons (blue) are injected along the axis of an intense dipole wave. In this field, the electrons will emit large amounts of high-energy photons (yellow). The polarization of the shown field is that of an electric dipole, with a poloidal electric field (red) and a toroidal magnetic field (green). (Figure is reprinted from [54].)

together with analytical estimates for the expected behavior of energetic electrons injected into this field, based on the LL equations of motion. In Sec. III we present the results of numerically modeling the interaction using the particle-in-cell (PIC) method together with QED modules [49]. First, we review the results of Ref. [54] on the high-energy photon production occurring at moderate laser powers. Second, we discuss the development of the shower-type cascade at high laser powers and identify different regimes possible within the range of $P < 10$ PW and initial electron energies less than 50 GeV. Third, we present results on efficient electron-beam-energy depletion, based on the analysis of the shower cascade. We conclude in Sec. IV and summarize where different regimes of interaction manifest themselves.

II. CLASSICAL MOTION IN A DIPOLE WAVE FIELD

In order to gain some qualitative picture of the role of radiation losses, we start by considering the classical form of radiation reaction and then discuss how the quantum effects, triggered by even stronger fields, modify this classical picture. The EM field of a dipole wave is a three-dimensional structure that in general can be described by an expansion in spherical harmonics around its point of focus. It is convenient to express this expansion in terms of transverse magnetic (TM) and transverse electric (TE) modes, which have toroidal magnetic and poloidal electric or poloidal magnetic and toroidal electric fields, respectively. The toroidal magnetic and electric fields can be written in spherical coordinates as [59]

$$\begin{pmatrix} B_\phi \\ E_\phi \end{pmatrix} = \begin{pmatrix} a_{\mathrm{TM}} \sin t \\ a_{\mathrm{TE}} \sin(t+\varphi_{\mathrm{TE}}) \end{pmatrix} \frac{J_{n+1/2}(R) L_n^1(\cos\theta)}{\sqrt{R}}, \tag{1}$$

where a_{TM} and a_{TE} are the amplitudes of the TM and TE modes, respectively, normalized to relativistic units $m_e\omega c/e$, φ_{TE} is the phase difference between the two modes, c is the speed of light, and m_e and e are the electron mass and charge, respectively. In addition, $J_\nu(x)$ is the Bessel function and $L_n^l(x)$ is the associated Legendre polynomial [60]. Time t is normalized to ω^{-1} and distance $R = \sqrt{x^2+y^2+y^2}$ is normalized to $k = c/\omega$. The poloidal components are readily obtained by making use of the relations between the Fourier components of the electromagnetic fields. The poloidal electric field in the TM mode is thus obtained from $\mathbf{E} = ik(\boldsymbol{\nabla} \times \mathbf{B})$ and the poloidal magnetic field in the TE mode from $\mathbf{B} = -ik(\boldsymbol{\nabla} \times \mathbf{E})$. For the analysis of electron motion, the field is however more conveniently expressed in cylindrical coordinates. For the nontrivial configuration of highest symmetry, with $n = 1$, we have

$$\begin{pmatrix} B_\phi \\ E_\phi \end{pmatrix} = \begin{pmatrix} a_{\mathrm{TM}} \sin t \\ a_{\mathrm{TE}} \sin t \end{pmatrix} \sqrt{\frac{2}{\pi}} \rho \left[\frac{\sin R - R\cos R}{R^3} \right], \tag{2}$$

where $\rho = \sqrt{x^2+z^2}$. The poloidal components of the electric and magnetic fields are in turn given by

$$\begin{pmatrix} E_\rho \\ B_\rho \end{pmatrix} = \begin{pmatrix} a_{\mathrm{TM}} \cos t \\ a_{\mathrm{TE}} \cos t \end{pmatrix} \sqrt{\frac{2}{\pi}} z\rho \left[\frac{3R\cos R + (R^2-3)\sin R}{R^5} \right] \tag{3}$$

and

$$\begin{pmatrix} E_z \\ B_z \end{pmatrix} = \begin{pmatrix} a_{\mathrm{TM}} \cos t \\ a_{\mathrm{TE}} \cos t \end{pmatrix} \sqrt{\frac{2}{\pi}} \left[\frac{(2z^2-\rho^2)R\cos R - (2z^2-\rho^2+\rho^2R^2)\sin R}{R^5} \right]. \tag{4}$$

The maximum of the TM (TE) mode is reached at the center of the dipole wave, with a value of $\sqrt{8/9\pi}\, a_{\mathrm{TM}}$ ($\sqrt{8/9\pi}\, a_{\mathrm{TE}}$), and is directed along the dipole axis.

A. Equations of electron motion

The motion of an electron in an EM field is described by the equations

$$\dot{\mathbf{p}} = \mathbf{E} + \mathbf{p} \times \mathbf{B}/\gamma + \mathbf{g}_{\mathrm{rad}}, \quad \dot{\mathbf{x}} = \mathbf{p}/\gamma, \tag{5}$$

where $\mathbf{x}$ and $\mathbf{p}$ are the electron position and momentum, respectively, and $\gamma = (1+\mathbf{p}^2)^{1/2}$ is the Lorentz factor. The momentum $\mathbf{p}$ is normalized to $m_e c$ and the fields are normalized to $m_e\omega c/e$. The radiation reaction force $\mathbf{g}_{\mathrm{rad}}$ can, for ultrarelativistic motion, be written in the Landau-Lifshitz form [61]

$$\mathbf{g}_{\mathrm{rad}} = -\frac{2\alpha a_S^2 \chi_e^2}{3\gamma}\mathbf{p}. \tag{6}$$

Here $\alpha = e^2/\hbar c \approx 1/137$ is the fine-structure constant, $a_S = m_e c^2/\hbar\omega$ is the normalized QED critical field, $\hbar$ is the reduced Planck constant, and the nonlinear quantum parameter χ_e is defined as $\chi_e = \sqrt{|F^{\mu\nu}p_\nu|^2}/a_S$ [16]. The EM-field tensor is defined as $F_{\mu\nu} = \partial_\mu A_\nu - \partial_\nu A_\mu$, where A_μ is the four-potential and $p^\nu = (\gamma, \mathbf{p})$ is the four-momentum of the electron. In three-dimensional notation the nonlinear quantum parameter reads

$$\chi_e = \frac{1}{a_S}\sqrt{(\gamma\mathbf{E} + \mathbf{p}\times\mathbf{B})^2 - (\mathbf{p}\cdot\mathbf{E})^2}. \tag{7}$$

It follows from Eqs. (6) and (7) that the expression for the radiation reaction force can be rewritten as

$$\mathbf{g}_{\rm rad} = -\epsilon_{\rm rad}\mathbf{p}\gamma\left[\left(\mathbf{E} + \frac{1}{\gamma}\mathbf{p}\times\mathbf{B}\right)^2 - \left(\frac{1}{\gamma}\mathbf{p}\cdot\mathbf{E}\right)^2\right], \tag{8}$$

where for later convenience we have introduced the dimensionless parameter $\epsilon_{\rm rad} = 2r_e/3\lambda\!\!\!^{-}$, with $r_e = e^2/m_e c^2 \approx 2.82\times10^{-13}$ cm the classical electron radius, $\lambda\!\!\!^{-}$ the reduced laser wavelength, and $\epsilon_{\rm rad} = 1.2\times10^{-8}$ for $2\pi\lambda\!\!\!^{-} = 1$ μm. The parameter $\epsilon_{\rm rad}$ characterizes how the radiation reaction affects the dynamics of a radiating electron.

In order to obtain analytical estimates for the electron energy under the influence of radiation reaction in a strong EM field, we turn to the simple case of an ultrarelativistic electron rotating in the antinode of a circularly polarized electromagnetic wave, with a normalized field amplitude a. In this scenario, in which $\gamma \sim a$, the power emitted is proportional to the fourth power of the electron's energy $m_e c^2\omega\epsilon_{\rm rad}\gamma^2(\gamma^2 - 1)$ [62]. Simultaneously, the electron can acquire energy from the electromagnetic field at a rate of $m_e c^2\omega a$. The steady-state condition of balance between the acquired and lost energy therefore yields $a^3 \approx \epsilon_{\rm rad}^{-1}$, with the result that radiation friction effects will become dominant in the limit of large EM-field amplitudes, when $a > a_{\rm rad} \equiv \epsilon_{\rm rad}^{-1/3}$. In this regime, and because of the energy loss, the electron energy is determined by (for further details see Ref. [62])

$$a^2 = (\gamma^2 - 1)\big(1 + \epsilon_{\rm rad}^2\gamma^6\big), \quad \tan\varphi = (\epsilon_{\rm rad}\gamma^3)^{-1}, \tag{9}$$

where φ is the angle between the directions of the electron momentum and the electric field. For $a \gg a_{\rm rad} = \epsilon_{\rm rad}^{-1/3}$ the energy of an electron ($\varepsilon = \gamma m_e c^2$) therefore scales as

$$\varepsilon \sim m_e c^2 (a/\epsilon_{\rm rad})^{1/4}, \tag{10}$$

which may also serve as a rough estimate for the electron energy in more general EM-field geometries.

B. Electron energy loss due to radiation reaction

An ultrarelativistic electron crossing a region of strong electromagnetic fields will lose energy due to radiation friction, the rate of which is easily obtained from the equations of motion to be

$$\dot\gamma = \frac{1}{\gamma}(\mathbf{p}\cdot\mathbf{E} + \mathbf{p}\cdot\mathbf{g}_{\rm rad}). \tag{11}$$

In order to emphasize the effects of radiation reaction, we consider the scenario of a strong field ($a \gg 1$) where the longitudinal component of the electron momentum dominates over the transverse component acquired in the EM field, meaning $p \gg a$. Writing the electron momentum as $\mathbf{p} = p\mathbf{e}_p$, the momentum equation takes the form

$$\dot p = -\epsilon_{\rm rad}p^2[(\mathbf{E} + \mathbf{e}_p\times\mathbf{B})^2 - (\mathbf{e}_p\cdot\mathbf{E})^2]. \tag{12}$$

For an electron moving parallel to the symmetry axis (z axis) of the MCLP configuration described by Eqs. (2)–(4), the equation can be further simplified to

$$p' = -\epsilon_{\rm rad}p^2K_z(\rho, z), \tag{13}$$

where the primed momentum denotes differentiation with respect to the coordinate z and the function $K_z(\rho, z) = (E_\rho - B_\phi)^2 + (E_\phi + B_\rho)^2$ governs the distribution of the radiation reaction force acting on the ultrarelativistic electron propagating in the z direction. We now assume that the field is an equal mix of the TE and TM modes $a_{\rm TE} = a_{\rm TM} = a_m$ with no phase difference $\varphi_{\rm TE} = 0$. With this choice, the peak field amplitude is related to the total laser power according to $a_0 = \sqrt{8/9\pi}\,a_m \approx 550\sqrt{P/1\ \text{PW}}$. The slightly lower peak amplitude for the EM dipole, compared to a purely electric or magnetic dipole, comes from the fact that the power is split equally between the two modes, reducing the peak amplitude at the center by $1/\sqrt{2}$. The K_z function then takes the form shown in Fig. 2. In particular, the function is equal to zero on the z axis, has a ρ^2 scaling for small radii $\rho \ll 1$, and reaches its maximum of $K_z \approx 0.24a_m^2$ at $\rho = \rho^\star \approx 2$ and $z = 0$. The maximum value of the nonlinear quantum parameter χ_e that can be achieved by an electron moving parallel to the z axis is $0.49\gamma a_m/a_S$. For an electron with initial momentum $\mathbf{p}_0$ and initial $\rho = \rho_0$, the solution to Eq. (13) is then given by

$$p(z) = \frac{p_0}{1 + (2/\pi)p_0\epsilon_{\rm rad}a_m^2\Phi(\rho_0, z)}, \tag{14}$$

where $(2/\pi)a_m^2\Phi(\rho_0, z) = \int_{-\infty}^{z} dz' K_z(\rho_0, z')$ [see Fig. 3(a)]. Although Eq. (13) is at the threshold of its applicability for the parameters chosen to plot the curves in Fig. 3(a), the evolution of the electron energy shows a rapid depletion and saturation. We may also note that for $(2/\pi)p_0\epsilon_{\rm rad}a_m^2\Phi(\rho_0, z) \gg 1$, the momentum $p(z)$ becomes independent of the initial momentum p_0, meaning that the particle in this highly dissipative system "forgets" about its initial conditions and its final momentum will tend to

$$p_\infty = \frac{\pi}{2\epsilon_{\rm rad}a_m^2\Phi(\rho_0, z = \infty)}. \tag{15}$$

For the approximations to be valid during the whole interaction process, the condition $p(z) \gg a_0$ must be satisfied, leading to the requirement that

$$a_0 \ll \left(\frac{4}{9\Phi(\rho_0, z)}\right)^{1/3}\epsilon_{\rm rad}^{-1/3}. \tag{16}$$

If satisfied, radiation reaction effects associated with the transverse motion should not play any significant role in the dynamics.

Based on the results for the final electron energy in the longitudinal (15) and transverse (9) motion in strong EM fields and in the presence of the radiation reaction, we may draw some conclusions on how the electron dynamics evolves with increasing EM-field power. We plot (15) and the solution of (9) in Fig. 3(b), revealing two intersecting curves. The value of a_0 at the intersection point scales as $a_0 = a_{\rm th} \sim \epsilon_{\rm rad}^{-1/3}$,

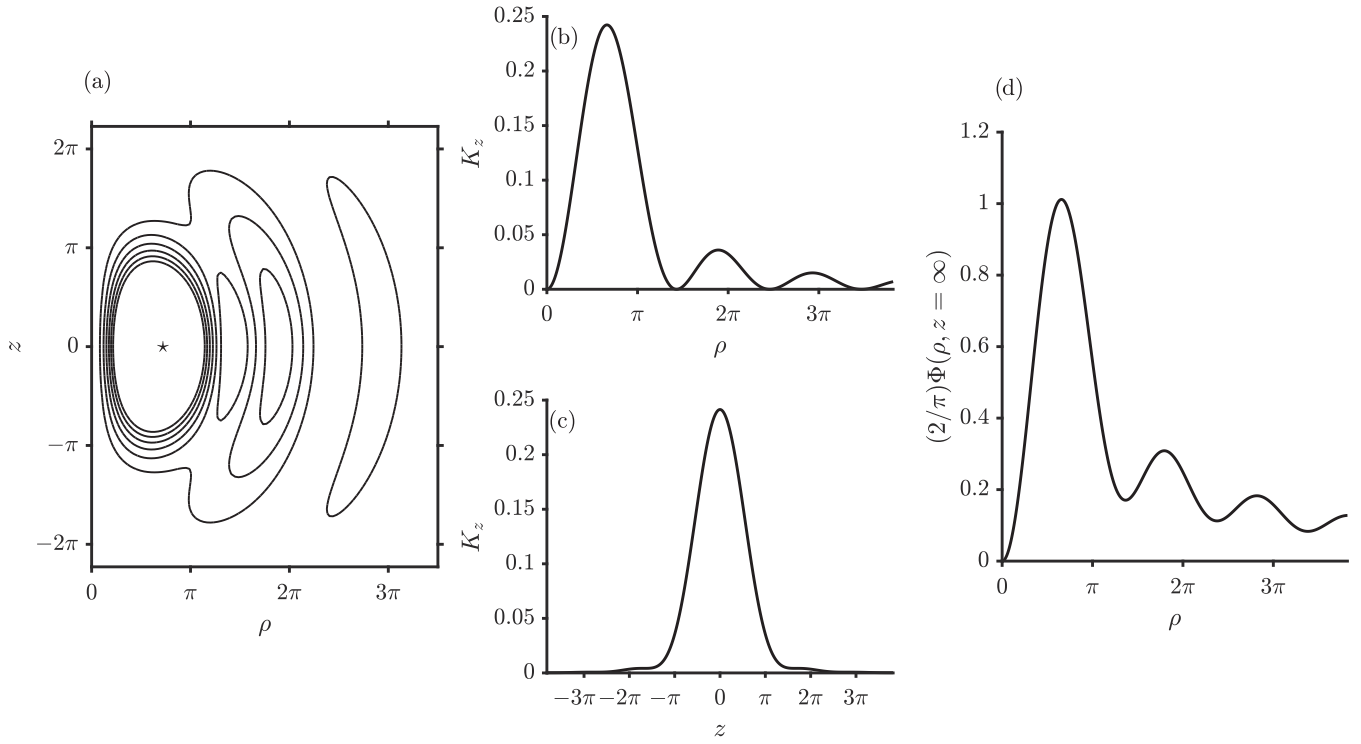

FIG. 2. (a) Isocontours of the function K_z in the (ρ), (z) plane. (b) Dependence of the function K_z on the radial coordinate ρ at $z = 0$. (c) Dependence of the function K_z on the longitudinal coordinate z at $\rho = \rho^\star \approx 2$. (d) Dependence of the function Φ on the radial coordinate ρ at $z = \infty$.

which corresponds to the threshold for the radiation effects becoming dominant in the transverse motion of an electron in an EM field (16). So, for electron-beam interaction with MCLPs with $a_0 < a_{\rm th}$, the emission of photons is mostly directed forward with electrons losing their energy down to (15), but not scattering to the sides. For $a_0 > a_{\rm th}$, the electrons will lose energy until the point where their transverse motion becomes important and reacceleration by the field can occur. In a strong field this motion is characterized by Eq. (9), which defines such electron motion, when the electron emits the same amount of energy it absorbs from the field per cycle. Moreover, the trapping phenomenon, which is connected to the existence of stable and quasistable trajectories in the field, is only possible for $a_0 > a_{\rm th}$. Thus, $a_{\rm th} \sim \epsilon_{\rm rad}^{-1/3}$ is the threshold between pure depletion and reacceleration.

In strong laser fields, the classical treatment of radiation losses becomes inaccurate in two specific ways. First, the overall rate of radiation losses will be suppressed, leading to the change of scaling from χ_e^2 to $\chi_e^{2/3}$. Second, the losses will have a probabilistic quantized form since the energy of emitted photons becomes comparable to the energy of the electron. Both these effects increase the probability of an electron to penetrate the strong-field region without the

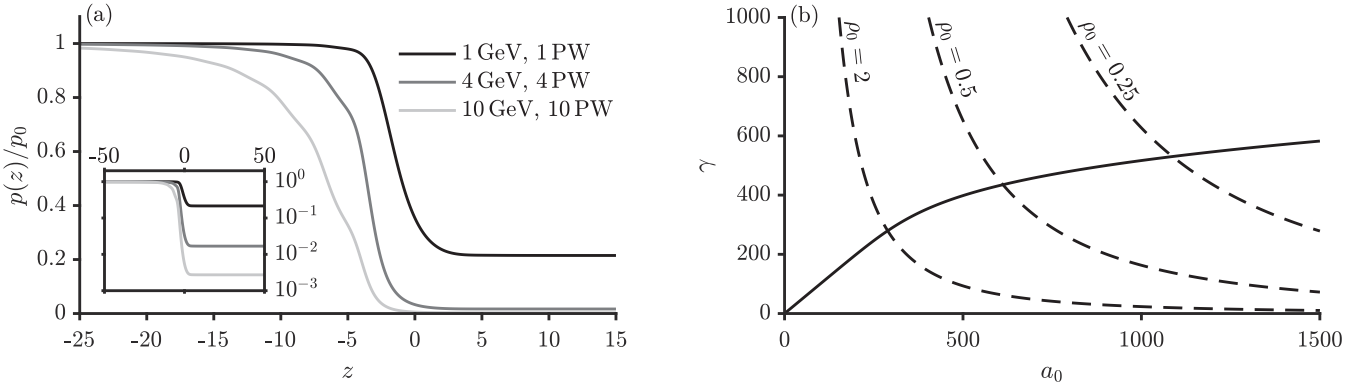

FIG. 3. (a) Evolution of the electron momentum in the EM dipole field according to Eq. (14) for $\rho_0 = 0.5$ and three sets of initial electron energy $\varepsilon_0 = \sqrt{p_0^2c^2 + m_e^2c^4}$ and laser power P. (b) Dependence of the electron energy on the peak amplitude a_0 of the EM field according to Eq. (9) (solid line) and Eq. (15) (dashed line) for three different values of ρ_0. The peak field amplitude is related to the laser power according to $a_0 = \sqrt{8/9\pi}\, a_m = 550\sqrt{P/1\ \text{PW}}$.

dramatic loss of its kinetic energy, in contrast to what is prescribed by the classical picture.

In what follows we test these conclusions in numerical simulations, employing strong-field QED formalism, i.e., the probabilistic nature of the photon emission by an electron and electron-positron pair production by a photon in a strong EM field. It can be expected that, at relatively low peak intensities of the MCLP configuration, an electron will lose part of its initial energy upon interacting with the EM field, but will mainly go through the field and emit photons along the direction of its propagation. At increasingly higher intensities electrons will be scattered more strongly sideways, which will also be reflected in the photon-emission directions. At very high intensities electrons will be scattered in all directions and therefore the photons will be emitted in a 4π angle. The energy of the electrons will in this case be characterized by Eq. (9). Furthermore, a_{th} should determine the optimal value for the energy depletion of the electron beam, since a_{th} is defined as the field strength at which the electron momentum acquires its minimum value.

III. INTERACTION ACCORDING TO THE QED PIC METHOD

To verify the obtained predictions and to analyze the interaction beyond the assumptions made, we turn to simulations based on the QED PIC code ELMIS [49]. We perform a set of simulations in which we vary the total incoming laser power P and the initial energy ε_0 of electrons passing through the dipole wave. The dipole wave contains equal parts electric and magnetic modes with no phase difference, as in Sec. II. It is generated at the boundary of the simulation box with a wavelength of $\lambda = 1$ μm and is supplied a constant (cycle-averaged) power. The dipole field is then formed through the self-consistent-field evolution, taking into account potential suppression due to pair cascades. The simulation box was divided into $128 \times 128 \times 128$ cells of $(\lambda/16)^3$ resolution, giving the simulation box a physical size of $8 \times 8 \times 8$ μm^3.

Electrons were injected into the simulation box in the form of a Gaussian-shaped electron bunch with an $L = 5$ μm FWHM longitudinal and $w = 1$ μm FWHM transverse size. The bunch is centered on and travels along the dipole axis with a total charge of 100 pC, corresponding to $N = 6.2 \times 10^8$ electrons. These values are similar to what is expected of electron bunches obtained from a laser wakefield accelerator (LWFA) (see Ref. [63] and references therein).

As the electrons interact with the EM field, photon emission and electron-positron pair creation are accounted for stochastically through the rates of the nonlinear Compton and multiphoton Breit-Wheeler processes. To keep the simulations computationally feasible, photons with an energy below $2m_ec^2$ are discarded as their chance of pair creation is minimal and therefore do not contribute further to the interaction dynamics. A particle thinning routine [64] is also employed in order to deal with the onset of pair cascades. The interaction is analyzed using data gathered on all particles inside the main interaction region, defined as a sphere of radius 3 μm centered at the dipole focus, and statistics are also captured on all particles leaving it. These data constitute the main results of this study and are described in more detail in the following sections.

The field structure described in Sec. II corresponds to a dipole pulse driven at a constant power. Since physical laser pulses are of finite energy and duration, the field structure can only be approximately described by Eqs. (2)–(4) for sufficiently long pulse durations. For more general temporal shapes, the field structure can most easily be obtained by generating the (incoming) field in the far-field region ($R \gg 1$) and then numerically advancing this field according to Maxwell's equations using a standard field solver (for analytical consideration of this problem see Ref. [28]). Thus, the electric mode of the dipole field can be generated in the far-field region using

$$\mathbf{B}^{ED} = \frac{3a_0}{2R}\sin(t+R)\Psi(t+R)[\hat{n}\times\hat{d}], \tag{17}$$

$$\mathbf{E}^{ED} = \frac{3a_0}{2R}\sin(t+R)\Psi(t+R)[\hat{n}\times[\hat{n}\times\hat{d}]], \tag{18}$$

where $\Psi(t+R)$ describes the temporal envelope of the pulse, $\hat{n} = \mathbf{R}/R$, and $\hat{d}$ is the (normalized) dipole vector, and similarly for the magnetic mode.

A. Source of high-energy photons

For the purpose of discussing the capabilities of the proposed source, we define a generation efficiency measure based on the total number of photons N_x that escape the interaction region with an energy above a given threshold ($\varepsilon_{\text{th}} = x\varepsilon_0$). In regimes where reacceleration is weak, an electron can emit at most one photon with an energy above $\varepsilon_0/2$, making $N_{1/2}/N$ a natural measure for high-energy photon generation as it also becomes bounded by 100%.

The photon generation efficiency is presented in Fig. 4 as a function of laser power and electron-beam energy for three different threshold energies. Since we consider a given dipole field configuration, we can quantify the entire field structure by a single parameter P without any additional assumptions on the focusing geometry.

For low thresholds [Fig. 4(a)] the measure effectively gives the total number of photons and shows that it increases with both laser power and electron-beam energy, as could be expected. For large thresholds [Fig. 4(b)] this trend is broken and an optimal laser power, for the purpose of high-energy photon generation, emerges. The explanation for this is found by considering the interplay between the Compton and Breit-Wheeler processes that both increase in rate with increasing field strengths. While this interplay initially favors an increasing production of high-energy photons, the fraction of high-energy photons able to escape the interaction region will eventually, for sufficiently large field strengths, start to decrease and instead fuel a shower-type cascade [65].

The efficiency for generating photons above half the initial electron-beam energy ($\varepsilon_{\text{th}} = \varepsilon_0/2$) is shown in Fig. 4(c). Similarly to Fig. 4(b), there is a region in which the efficiency initially increases with increasing laser power, but eventually drops off as the photon decay into pairs begins to dominate. What is even more interesting is that the optimal laser power is almost completely flat around a relatively moderate 0.4 PW for a large range of electron energies, with an efficiency of

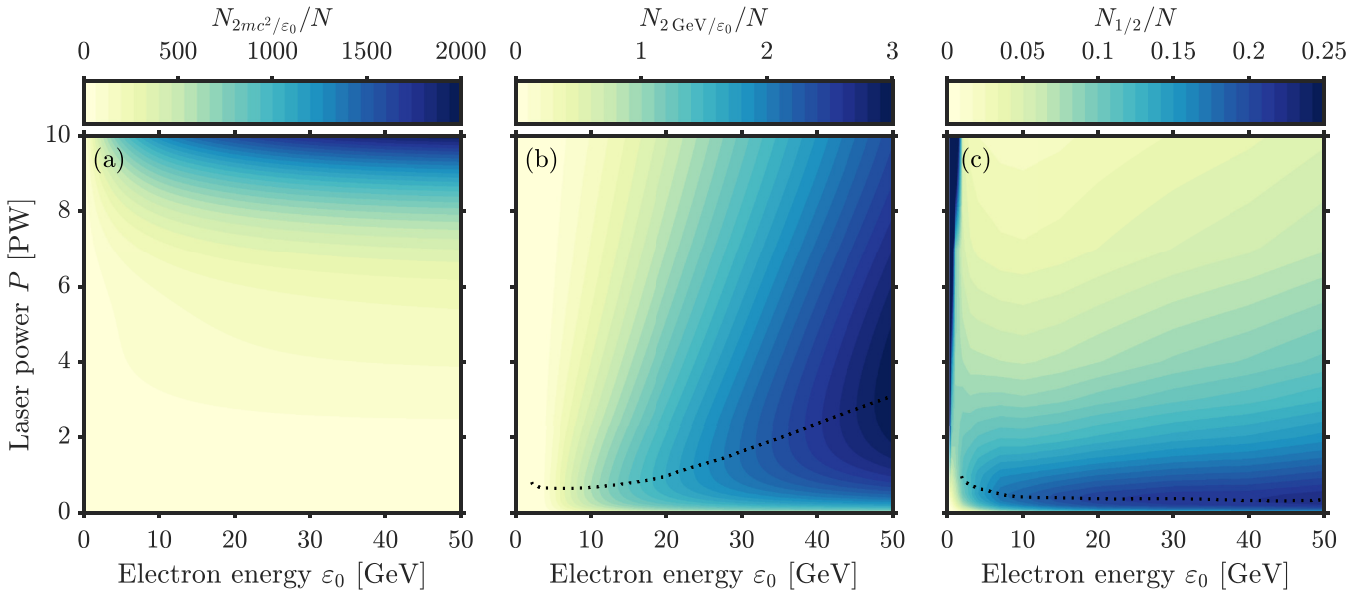

FIG. 4. Total number of photons, normalized to the initial number of electrons in the beam ($N_{\varepsilon_{\mathrm{th}}/\varepsilon_0}/N$), detected above an energy threshold $\varepsilon_{\mathrm{th}}$ of (a) $2mc^2$, (b) 2 GeV, and (c) $\varepsilon_0/2$ at the end of the simulation. In (b) and (c) the dotted lines indicate the optimal laser power as a function of electron energy.

$\sim$20%. The efficiency was more generally shown in Ref. [54] to depend on the field shape and field structures with the greatest intensity gradients were shown to be superior.

The flatness in optimal power in Fig. 4(c) can also be explained by analyzing the probability of the emission of high-energy photons through the Compton process. The differential emission rate in this case is [26]

$$dP^e = -\frac{\alpha}{\pi\lambda_C}\frac{m_e}{\gamma}\left(\int_z^\infty \Phi(z')dz' + \frac{y}{z}\Phi'(z)\right)d\varepsilon_\gamma. \qquad (19)$$

Here $\Phi(z)$ and $\Phi'(z)$ are the Airy function and its derivative, respectively, which can be expressed in terms of the modified Bessel function of the second kind, $\Phi(z) = 3^{-1/2}\pi^{-1}z^{1/2}K_{1/3}(2z^{3/2}/3)$ and $\Phi'(z) = -3^{-1/2}\pi^{-1}zK_{2/3}(2z^{3/2}/3)$, and

$$z = \left[\frac{\varepsilon_\gamma}{(1-\varepsilon_\gamma)\chi_e}\right]^{2/3}, \quad y = 1 - \varepsilon_\gamma + \frac{1}{1-\varepsilon_\gamma}, \qquad (20)$$

where ε_γ is the emitted photon energy normalized to its maximum value. The dependence of the number of high-energy photons on the initial electron energy can then be calculated as $P^e_{1/2}(\gamma) = \int_{1/2}^1 dP^e$, which demonstrates an almost flat behavior for 0.4-PW laser power and electron energies in the (10–100)-GeV range.

The second high-efficiency region that can be seen in Fig. 4(c), for $\varepsilon_0 \lesssim 1$ GeV, is a direct result of reacceleration, which makes multiple emission of photons with an energy greater than $\varepsilon_0/2$ possible. While this regime lends itself to larger numbers of such photons, their energies are, as previously discussed, relatively low as they are limited to only a few GeV.

In Fig. 5 we compare the capabilities of the source to both existing and previously proposed sources. Assuming an optimal laser power of 0.4 PW and a 10- or 50-GeV electron beam, with a physical size and total charge as specified in Sec. III, the source is shown to be able to provide a peak brilliance [Fig. 5(a)] similar to that of the avalanche-cascade source [33] but at greater photon energies. For 10 GeV (50 GeV) the peak brilliance is estimated to 10^{26} photons/s mrad^2 mm^2 0.1% bandwidth at 250 MeV (370 MeV). In comparing it to other Compton sources, it is also instructive to compare them in terms of average flux [Fig. 5(b)]. Assuming a repetition rate of 1 Hz, the proposed source is comparable to current facilities in terms of average flux, but is able to reach greater energies. While these aspects allow us to compare the source to others it fails to capture what is perhaps the most interesting aspect of the dipole sources, namely, that the high-energy photons are produced in dense bunches on the order of 10^{20} cm^{-3}.

B. Onset and occurrence of pair cascades

When an energetic electron beam interacts with a strong EM field its energy is converted into secondary electrons, positrons, and photons in a process commonly referred to as a cascade, which can be of either shower or avalanche type. The shower type corresponds to the case where the initial energy of particles (or photons) entering the strong field region is driving the cascade, whereas the avalanche type corresponds to the case where the energy of particles participating in the cascade is continuously replenished through their repeated acceleration by the same strong field. Because both types involve a production of electron-positron pairs, characterizing the interaction by the number of pairs produced can therefore give an indirect estimate of the strength of the cascade.

For low initial energies, the electron dynamics is dominated by the influence of the much stronger field ($\gamma \ll a_0$). As the electrons rapidly lose their initial inertia they can get trapped in this field, where they produce pairs through their reacceleration followed by emission of high-energy photons,

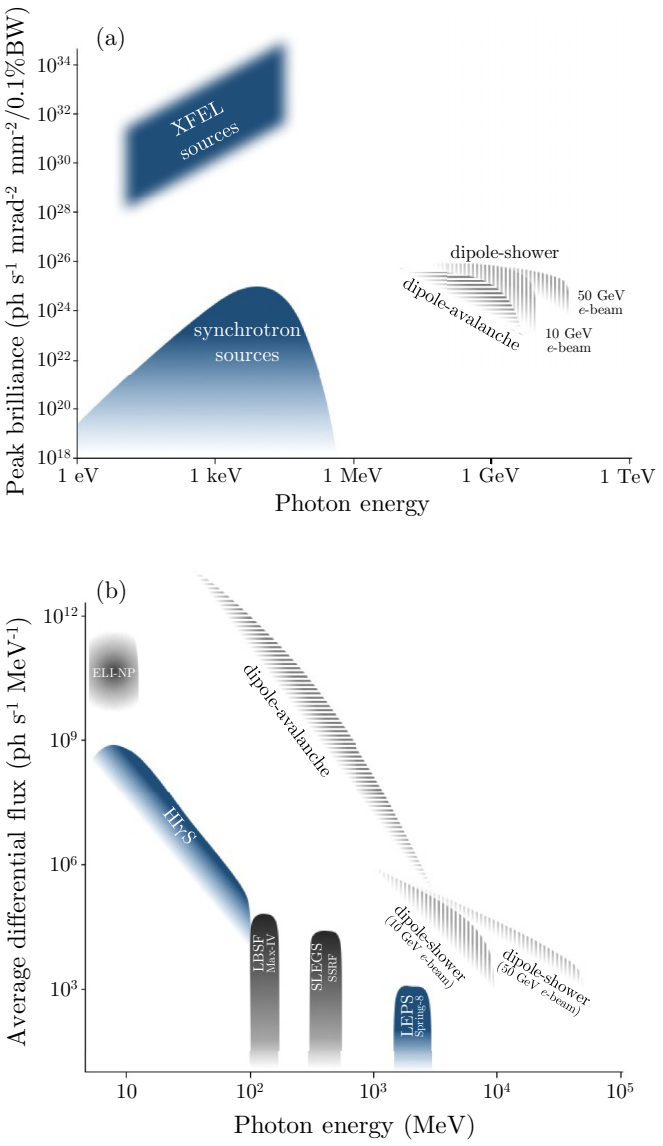

FIG. 5. Comparison of the dipole source with existing sources, in terms of (a) peak brilliance and (b) average flux. The plots schematically illustrate the properties of existing (blue) as well as upcoming or planned (solid gray) facilities. The gray hatched areas show the prospective properties of the dipole-avalanche source (horizontal) and our proposed source (vertical), the dipole-shower source. Here XFEL denotes x-ray free-electron laser.

initiating an avalanche-type cascade. Due to the probabilistic nature of the QED processes, it becomes possible to observe a notable yield in high-energy photon production well below the values of P required for the dominant appearance of the trapping. As this trapping becomes self-sustained, the comparison becomes formally inconsistent because the number of particles produced inside and emitted from the dipole field continues to grow until the end of the simulation, necessitating a comparison that takes the finite duration of the laser field into account. In the case of an electric dipole, the avalanche cascade becomes self-sustained for $P_{\rm min} \simeq 7.2$ PW [33], but for the electromagnetic dipole studied here this threshold is increased to beyond 10 PW. This fact is evident in the absence of a significant pair production in conjunction with the efficient photon production. Nevertheless, as will made apparent in the subsequent discussion, this regime exhibits most other features of a cascade, leading us to signify it as an *avalanche precursor*.

For larger values of initial energy ($\gamma \gtrsim a_0$) this avalanche precursor no longer appears. This is because both the injected and the produced particles particles have a large enough inertia to penetrate the high-field region before depleting their energy and getting trapped. As was discussed in Sec. III A, the onset of a shower cascade ultimately hampers the yield of high-energy photons in favor of an increasingly larger production of pairs. This becomes clear upon comparing Figs. 4(b) and 4(c), showing the number of high-energy photons produced, with Fig. 6(a), showing the total number of produced pairs. While the high-energy photon production for $\varepsilon_0 \gtrsim 1$ GeV and $P \gtrsim 1$ PW drops with increasing laser power, an increase in either parameter consistently results in a larger number of electron-positron pairs. The regimes of efficient high-energy photon production and efficient pair production are therefore clearly separated in the parameter space and it becomes possible to generate as many as 20 (40) times the initial number of electrons, at 10 PW and 10 GeV (50 GeV).

Neglecting the effects of transverse motion and assuming that the electron dynamics is fully determined by the depletion of the electron energy, the sum of the energy of all particle species is approximately equal to the initial beam energy. This is in principle how the notion of the shower-type cascade is defined, that the energy supplied to the cascade comes almost exclusively from the initial particle beam. In our simulations we tracked the evolution of the total energy carried by each particle species. It was found that for most values of initial electron energy and laser power the sum of these energies at the end of the simulation is approximately equal to the total energy initially carried by the electron beam. However, when the laser power approaches 10 PW, this changes significantly [see Fig. 6(b)]. While the combined energy of all the electrons and positrons at the end of the interaction is either approximately equal to or smaller than the energy initially carried by the beam, for most values of ε_0, the total energy carried away by the emitted photons can significantly exceed that of the initial beam. This becomes especially pronounced for lower values of ε_0, with 12 times the initial energy being emitted as photons in the case of 1 GeV compared to 2.6 times the initial energy in the case of 50 GeV (both at 10 PW). This indicates that a significant reacceleration begins to develop as we approach 10 PW, especially at low ε_0, as the added energy can only come from the laser field.

To further strengthen this view, we may look at the energy partitioning between the different species at the end of the simulation, shown in Fig. 7. At 1 GeV and 1 PW [Fig. 7(a)] the electron beam loses 61% of its energy in the interaction such that the electrons and photons in the end carry $0.39E_0$ and $0.62E_0$, respectively, while the energy of the positrons is negligible. This means that the electron-beam energy is the predominant source of energy, while a small additional amount comes from the acceleration of particles in the EM field. A similar picture can be seen at 4 GeV and 4 PW [Fig. 7(b)]. Here the electron beam loses 94% of its energy

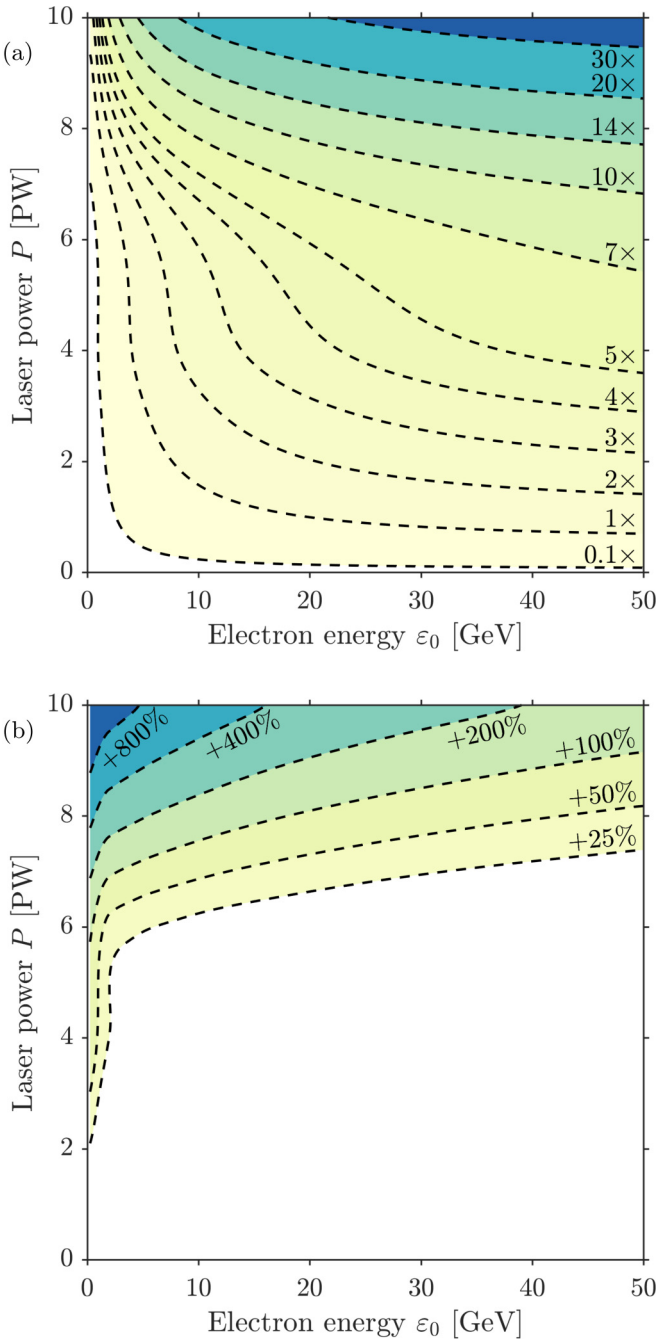

FIG. 6. Dependence of (a) the number of generated electron-positron pairs relative to the initial number of electrons in the beam (N) and (b) the total energy carried by all particles at the end of the simulation relative to the initial energy carried by the electrons in the beam, on the initial electron energy and laser power.

in the interaction, while photons and electron-positron pairs in the end carries $0.97E_0$ and $0.14E_0$, respectively. The final energy, therefore, amounts to $1.2E_0$, where the additional $0.2E_0$ comes from the EM field. As we approach 10 PW the interaction becomes qualitatively different, with significantly more energy carried by photons than by electrons and positrons. Furthermore, while the total photon energy quickly saturates for lower values of P, this saturation gets significantly delayed around 10 PW and the emitted photon energy can be seen to increase until the very end of simulation at 80 fs.

This change in behavior is, as already mentioned, connected to a partial trapping of a few charged particles, which exceed the time it usually takes to escape the strong-field region. In this state, they move along quasistable orbits and radiate away the excess energy gained from the field, giving rise to the demonstrated extraction of energy from the field despite the absence of a fully self-sustained cascade. A qualitative explanation is provided by the analysis presented in Sec. II B. If $a < a_{\text{th}}$ then the electrons lose energy down to the value roughly given by Eq. (15), with photon emission mainly directed forward. However, if $a > a_{\text{th}}$ then the transverse motion of the electrons will become increasingly more important as they lose energy until it is roughly determined by Eq. (10), where the losses are balanced by reacceleration. Due to the transverse nature of this motion, photons (as well as pairs) will be emitted in all directions, as seen in Fig. 8, and with an energy roughly on the order of $m_e c^2 (a/\epsilon_{\text{rad}})^{1/4}$, as obtained in Eq. (10).

C. Radiation-dominated electromagnetic shield

As shown previously in this section, a prolific production of photons occurs as the laser power approaches 10 PW. These photons account for the largest contribution to the total energy of the final particles, which can significantly exceed the initial beam energy. At 10 PW the electrons and positrons, while temporarily trapped in the field, provide an effective mechanism for transforming laser energy into γ-ray photons. In Sec. II B the energy loss of a high-energy electron injected into the field is studied on the basis of classical radiation reaction, suggesting that an electron beam can be effectively stopped over micron-size distances, as it radiates away most of its energy. This deceleration, according to Eq. (15), improves with increasing laser power. However, as we have seen, when the laser power is increased there is also a large production of photons and pairs. For this radiation shield to be considered effective it is therefore important that the generated particles have significantly lower energies than the electrons initially in the beam.

The expected electron energy as a function of longitudinal coordinate is presented in Fig. 3(a), showing a rapid energy loss over about a wavelength of propagation distance. The corresponding quantity from the simulations is the average energy of the initial beam electrons presented in Fig. 7 (blue dotted lines), but here as a function of time. Although these simulations were performed with an electron beam of finite length, it shows a very similar trend, centered around 40 fs, where the broadening can explained by the ∼15-fs duration of the electron beam. This general monotonic trend can be seen to persist even in cases where the trapping of particles causes a significant generation of electron-positron pairs, as seen in Fig. 7(c).

The energy spectra of electrons, positrons, and photons at the end of the simulation are shown in Fig. 9 for a few different laser powers and electron energies. While the total amount of energy carried by all species was demonstrated earlier to increase with laser power, the average energy of

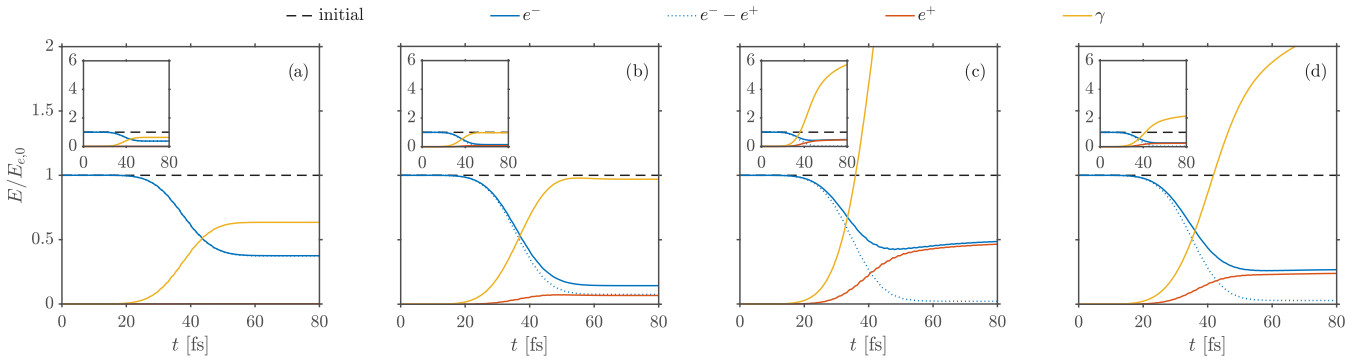

FIG. 7. Temporal evolution of the total energy, partitioned between electrons [blue (upper gray) line], positrons [red (lower gray) line], and photons [yellow (light gray)] for different values of laser power P and initial electron beam energy ε_0: (a) 1 PW and 1 GeV, (b) 4 PW and 4 GeV, (c) 10 PW and 10 GeV, and (d) 10 PW and 50 GeV. The total energy of the initial electron beam (dashed line) and the total energy carried by the electrons originating from the initial beam (blue dotted line) are also shown. Insets represents the same data with a greater vertical scale.

the electrons is shown here to decrease at the same time. This remains true for a large range of parameters and the electron and positron spectra can be seen to peak at lower values (below 200 MeV) at high power, despite much greater initial electron energies. The final average energy (relative to the initial energy ε_0) of electrons is also presented in Fig. 10(a) [Fig. 10(b)], further demonstrating how the average energy decreases with increasing laser power. The only deviation from this trend can be found at low ε_0, around the avalanche precursor, where the reacceleration contributes to an increased average energy.

Since the average electron energy for large laser powers becomes strongly dominated by the energy carried by the generated pair plasma, it is also instructive to look at the average electron energy of the electrons originating from the beam, excluding the electrons produced during the interaction, presented in Fig. 11. While this figure in general shows the same trend as in Fig. 10(b), there are mainly

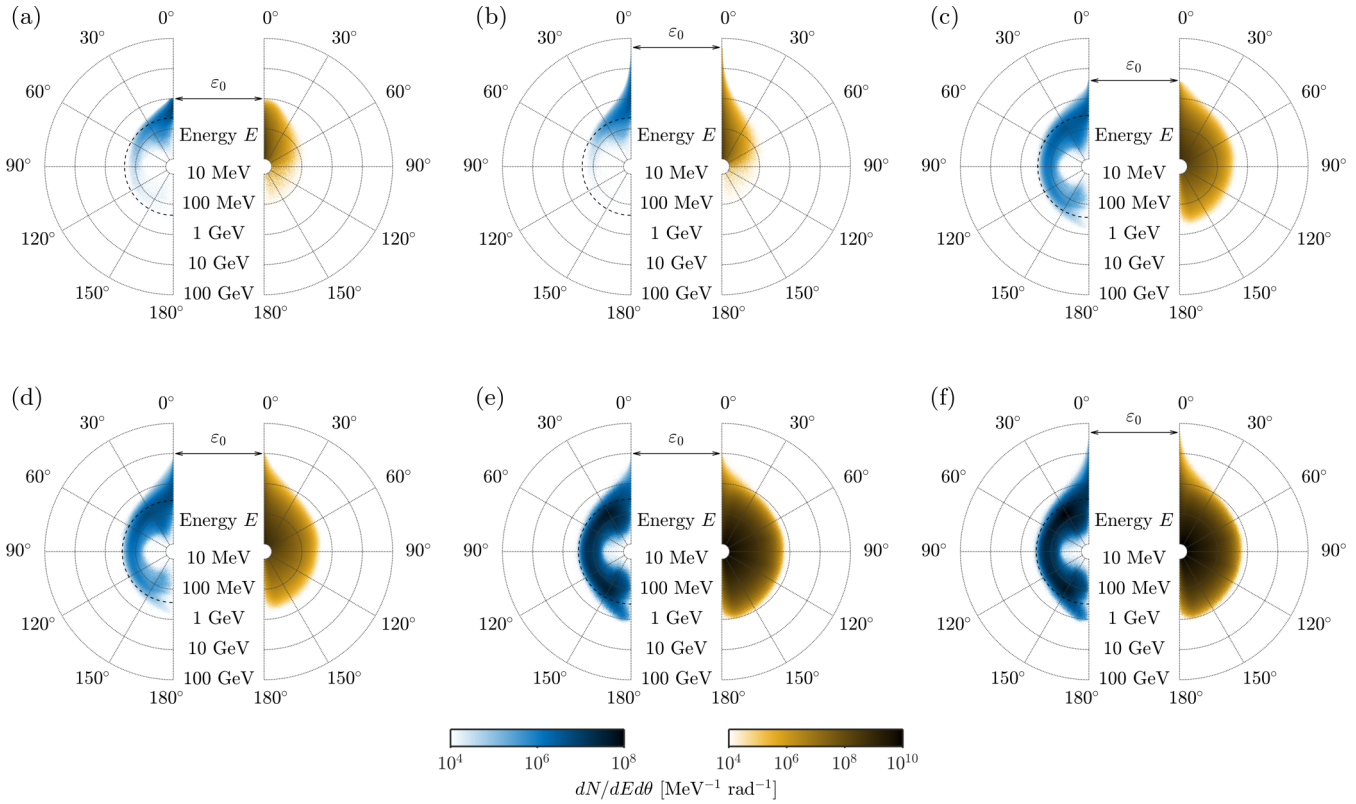

FIG. 8. Energy-angle distributions of electrons (blue, left) and photons (yellow, right) emitted from the interaction for six cases of laser power P and initial electron energy ε_0: (a) 1 PW and 1 GeV, (b) 1 PW and 50 GeV, (c) 4 PW and 4 GeV, (d) 4 PW and 10 GeV, (e) 10 PW and 10 GeV, and (f) 10 PW and 50 GeV.

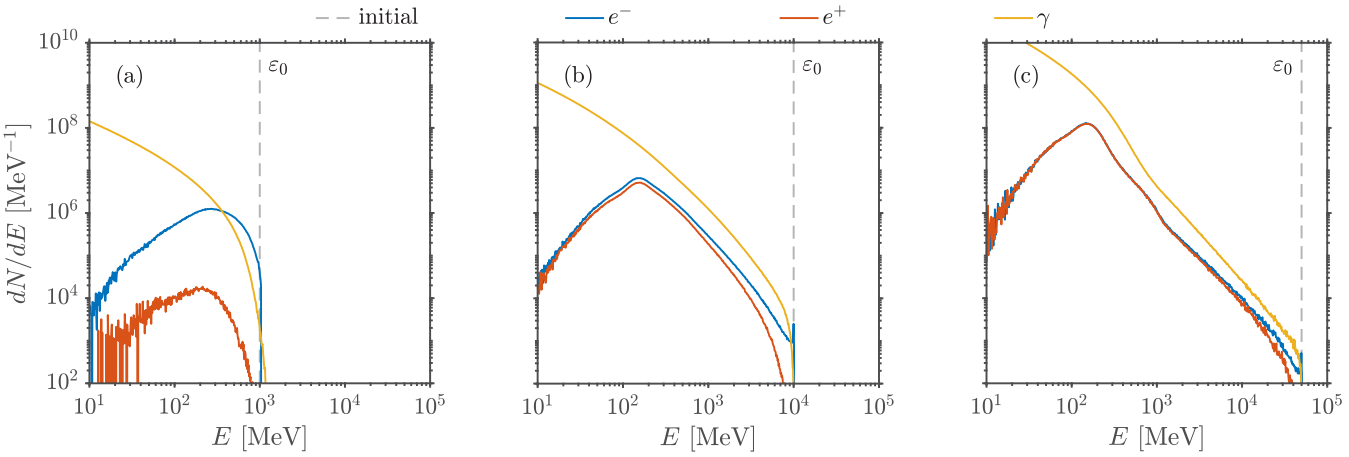

FIG. 9. Energy spectra of electrons [blue (upper gray) line], positrons [red (lower gray) line], and photons [yellow (light gray) line] at the at the end of the simulation for three different cases of laser power P and initial electron energy ε_0: (a) 1 PW and 1 GeV, (b) 4 PW and 10 GeV, and (c) 10 PW and 50 GeV. Also marked is the initial electron energy ε_0 (dashed gray line).

two things worth noting. First, the average energy of the beam electrons is greater than that of the entire ensemble, in practically all of the studied parameter space. Second, for a given laser power, the average energy can here be seen to increase with increasing initial energy, after a certain point. This is a direct consequence of the quantum suppression of radiation reaction. As the typical χ_e experienced by the electrons increases beyond unity, the average radiation loss scaling of χ_e^2 is suppressed to $\chi_e^{2/3}$. The average radiation loss, as a ratio over the initial particle energy, therefore decreases with increasing ε_0, causing the shift in scaling seen in Fig. 11 at large ε_0.

In terms of numbers, a 1-GeV electron beam subject to a total MCLP laser power of 0.5 PW loses roughly 50% of its initial energy, which is similar to the results of recent experiments on radiation reaction [6,7]. This energy depletion rapidly increases with increased laser power, going as high as 98% for 15 GeV and 10 PW. While the energy losses decrease with increasing initial electron energy due to quantum suppression, this dependence is weak and the depletion is therefore almost constant for electron energies from 5 to 50 GeV, for fixed laser power.

D. Electromagnetic field depletion

At extremely high intensities the electron-beam-energy depletion discussed in Sec. III C may in principle be accompanied by depletion of the EM field, as detailed in Refs. [66,67]. Over the course of the multiphoton Compton and Breit-Wheeler processes, which are responsible for transforming the initial electron-beam energy into photons and electron-positron pairs, a significant number of photons are absorbed from the EM field. The interaction of an electron beam of sufficiently high charge with an intense EM field can therefore lead to depletion of the field energy. Given the high intensities achievable with the setup considered in this paper, it is not unthinkable for such a scenario to manifest itself. Based on the results of Ref. [67], we estimate that for the field depletion to amount to a sizable contribution to the interaction of a 10-PW MCLP field and a 500-MeV (50-GeV) electron beam, the number of particles in the beam should be 10^{13} (10^{11}). For a 100-pC electron beam in the energy range studied in this paper, the peak field of the MCLP setup must exceed the Schwinger field in order for the field depletion to become significant. Given the parameters considered here, the interaction therefore does not allow for field depletion to manifest itself.

IV. CONCLUSION

In this paper we studied the interaction of a relativistic electron beam with multiple-colliding laser pulses. This interaction is highly nonlinear and is further complicated by the dynamic interplay of strong-field QED effects. We showed that, depending on the interaction parameters, initial electron energy, and laser power, the interaction can demonstrate a number of different regimes: (i) production of dense beams of high-energy photons, (ii) triggering shower-type cascades for reaching extreme states of generated electron-positron plasmas, and (iii) electron-beam-energy depletion. These regimes, summarized in Fig. 12 in a map over the studied parameter space, are the result of the balance in relative strength between the separate processes.

For low-electron-beam energies, the dynamics is shown to be dominated by the deflection and acceleration of the particles in the strong field. For increasingly greater field intensities, particles are trapped in the field focus for longer periods of time, giving rise to an avalanche precursor that becomes self-sustained at yet higher intensities, as discussed in Sec. III A. The trapping provides an efficient source of both electron-positron pairs and high-energy photons, but because the particle energies is limited by the reacceleration provided by the field, this regime has a reduced efficiency for producing photons with energies above a few GeV.

At high initial electron energies, multi-GeV photons can be efficiently produced. This efficiency is optimal around 0.4 PW, as greater laser intensities shift the balance between the Compton and Breit-Wheeler processes in favor of pair production, hampering the photon yield for the benefit of a shower cascade. As shown in Ref. [54], the remarkable localization of the field provided by the dipole wave plays a

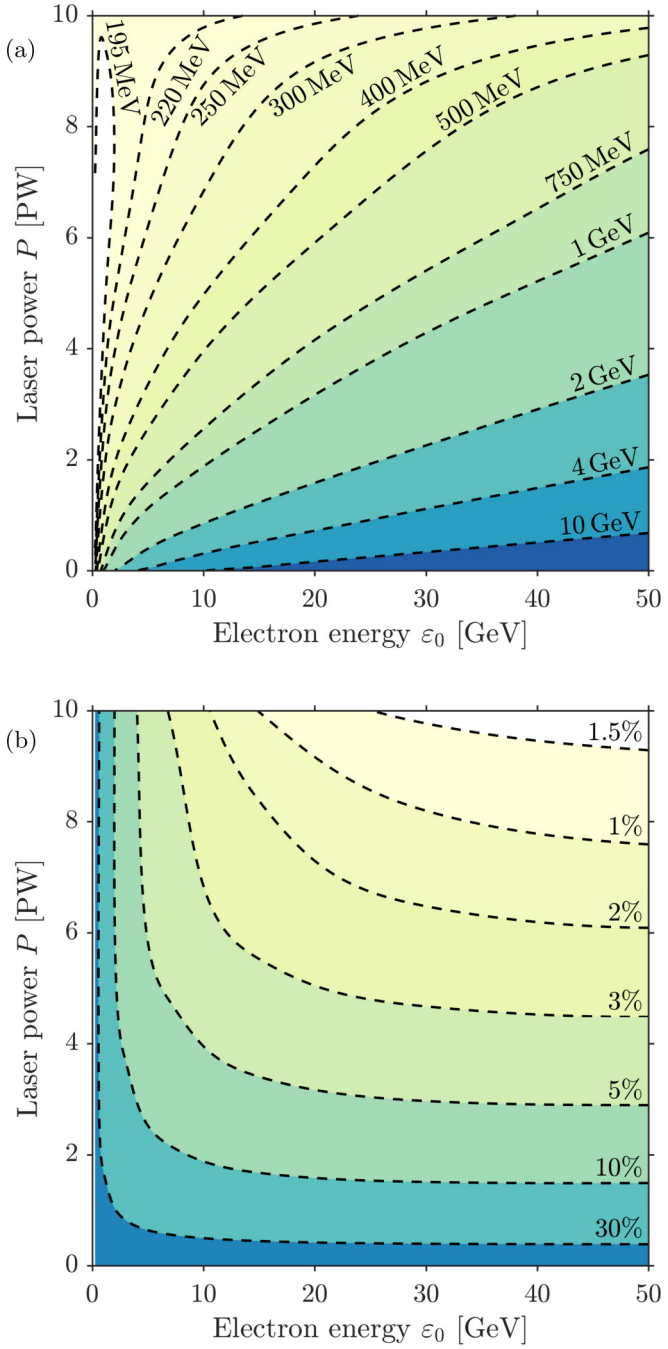

FIG. 10. (a) Final average electron energy and (b) final average electron energy relative to the initial electron energy ε_0, as functions of ε_0 and laser power P. The averages are computed accounting for all electrons, originating both from the initial beam and from pair creation.

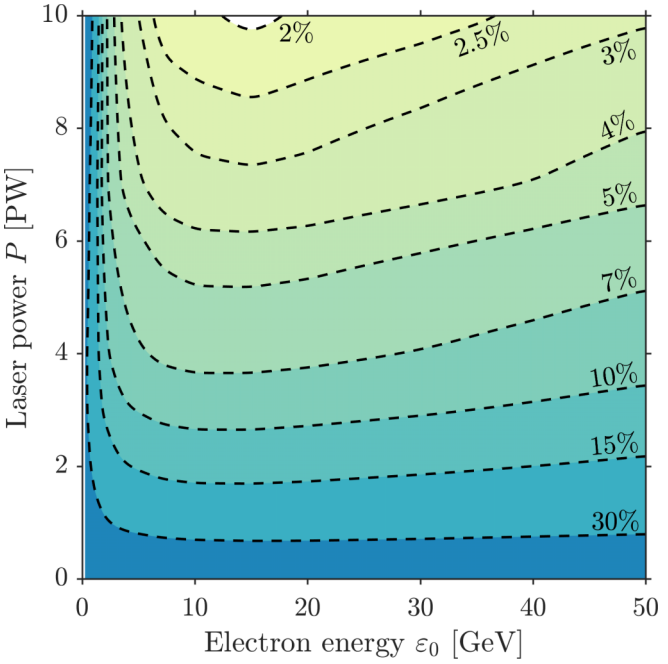

FIG. 11. Average electron energy relative to the initial electron energy ε_0, shown as a function of ε_0 and laser power P. The averages are computed accounting only for the electrons originating from the initial beam.

crucial role in attaining this balance at low laser power and for achieving an overall high efficiency of the high-energy photon production. We compared here the capabilities of the source to existing and previously proposed sources (see Fig. 5). It is shown to be able to provide a peak brilliance and average flux similar to conventional synchrotron sources, but at greater photon energies. Another important aspect of this source is the fact that the photons are generated in bunches of high density ($\sim 10^{18}$ cm^{-3} using LWFA bunches), clean from heavy charged particles and neutrons, naturally accompanying bremsstrahlung sources. It also provides the possibility to create beams with at least a partial polarization of photons, by letting the electron beam pass the focused field off-center such that the radial acceleration of electrons leads to the presence of a predominant polarization direction. This can be important for experiments, e.g., on Delbrück scattering [68].

Two more regimes can be identified at high intensities. First, the shower-type cascade, discussed in Sec. III B, occurs when the energy of an electron beam is predominantly transformed into electron-positron pairs. As the high-energy electrons of the initial beam enter the dipole field, they begin to lose energy through multiple emissions of photons. These photons then decay into electron-positron pairs, which themselves have enough energy to emit photons. At about 8 PW the number of electron-positron pairs is an order of magnitude larger than the initial number of electrons and this number increases rapidly with both increasing laser power and initial electron energy. Second, the large emission of photons at high intensities suggests a fast depletion of the electron-beam energy. In Sec. II B the field structure is predicted to be able to effectively stop the electron beam over about a wavelength of propagation distance. As discussed in Sec. III C, the electron energy losses are maximized for high intensities and around 15 GeV, with as much as 98% of the initial energy being radiated away. The occurrence of an optimal initial energy comes from the fact that the quantum suppression of radiation emission reduces the relative energy losses at sufficiently large initial electron energies ($\gtrsim$15 GeV), as the average energy loss shifts from a χ_e^2 to a $\chi_e^{2/3}$ scaling.

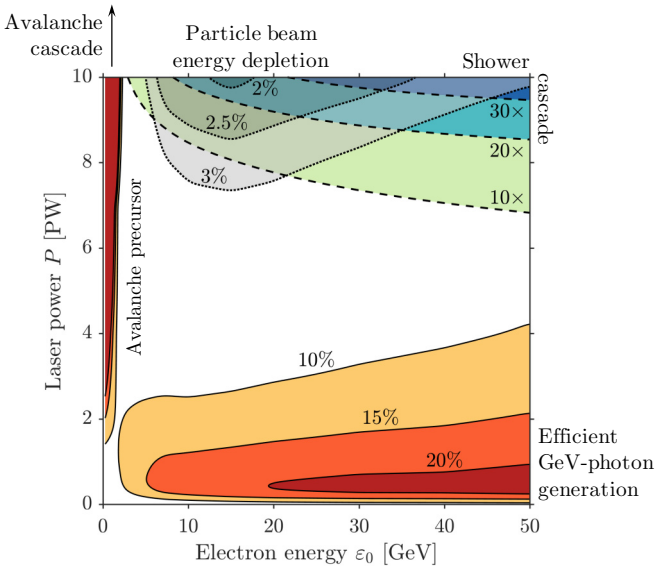

FIG. 12. Occurrence of different regimes in the interaction of a high-energy electron beam with MCLP in the parameter space of initial electron energy ε_0 and total laser power P: (i) high-energy photon generation [contours of the number of high-energy photons normalized to the number of initial electrons (solid)], (ii) shower-type cascade [contours of the number of e^-e^+ pairs normalized to the number of initial electrons (dashed)], and (iii) electron-beam-energy depletion [contours of the final electron-beam energy as percentage of the initial electron-beam energy (dotted)]. The contours of efficient high-energy photon generation occupy two separate regions: (1) the efficient generation of multi-GeV photons using electron beams of high energy and (2) an avalanche precursor, characterized by a partial trapping and reacceleration of particles, providing efficient generation of few-GeV photons.

The studied regimes of interaction outline a range of opportunities accessible for one or a few petawatt laser facilities augmented by the MCLP concept. One of the most apparent and crucial feasibility aspects for these experimental objectives is the requirement on the point stability and on the degree of synchronization of the laser pulses [69,70]. Although a dedicated analysis must be based on a concrete choice of experimental design, we can outline a qualitative argument on that matter. In the considered scenarios we neither observe nor exploit any phase-sensitive particle dynamics, such as anomalous radiative trapping (ART) [34]. Instead, we only utilize the fact that a high-field intensity is reached over the distance of about one wavelength. In addition, we consider perhaps the most insensitive (in this aspect) case of an *electromagnetic* dipole wave. This implies that the point stability has to be around one wavelength, whereas the temporal synchronization only requires an overlap of the laser pulses when they reach the central point. Note that the implementation of the MCLP concept for these experiments can play an important role in forming a staged program towards more demanding, phase-sensitive interaction scenarios triggered by the ART. For example, although the spatial and temporal mismatches of about several percent do not impede the ART dynamics, the yield of high-energy photons and leptons drops under such conditions by several tens of percent and therefore the source would largely benefit from further reduction of such mismatches [33].

To conclude, in this paper we showed that the high-field MCLP configuration together with high-energy electron beam not only provides an advantageous framework for studying strong-field QED phenomena, but also demonstrates the ability of this configuration to advance possible applications, in particular, as a source of high-energy photons. We showed that the MCLP configuration makes it possible to study strong-field QED phenomena starting from single-emission processes to multistaged ones involving significant transformation of laser energy into emerging electrons, positrons, and photons. This is why the outlined prospects of using the MCLP configuration, together with previous theoretical findings [25,29,31–34,41,52,53], provide a strong motivation for implementing more advanced and challenging focusing geometries, such as the dipole wave, in order to make better use of the produced laser radiation at large-scale laser facilities.

ACKNOWLEDGMENTS

J.M. would like to thank T. G. Blackburn for helpful discussions. S.S.B., C.G.R.G., C.B.S., and E.E. acknowledge support from the U.S. DOE Office of Science Office of HEP under Contract No. DE-AC02-05CH11231. J.K.K. acknowledges support from JSPS KAKENHI Grant No. 16K05639. S.V.B. acknowledges support at the ELI-BL by the project High Field Initiative (Grant No. CZ.02.1.01/0.0/0.0/15 003/0000449) from the European Regional Development Fund. The research was partly supported by the Ministry of Education and Science of the Russian Federation under Contract No. 14.W03.31.0032 (A.G.), by the Swedish Research Council Grants No. 2013-4248, No. 2016-03329 (M.M.), and No. 2017-05148 (A.G.), and by the Knut and Alice Wallenberg Foundation (A.G., J.M., and M.M.). The simulations were performed on resources provided by the Swedish National Infrastructure for Computing at HPC2N.

[1] G. A. Mourou, T. Tajima, and S. V. Bulanov, Rev. Mod. Phys. **78**, 309 (2006).

[2] M. Marklund and P. K. Shukla, Rev. Mod. Phys. **78**, 591 (2006).

[3] A. Di Piazza, C. Müller, K. Z. Hatsagortsyan, and C. H. Keitel, Rev. Mod. Phys. **84**, 1177 (2012).

[4] C. Bula, K. T. McDonald, E. J. Prebys, C. Bamber, S. Boege, T. Kotseroglou, A. C. Melissinos, D. D. Meyerhofer, W. Ragg, D. L. Burke, R. C. Field, G. Horton-Smith, A. C. Odian, J. E. Spencer, D. Walz, S. C. Berridge, W. M. Bugg, K. Shmakov, and A. W. Weidemann, Phys. Rev. Lett. **76**, 3116 (1996).

[5] D. L. Burke, R. C. Field, G. Horton-Smith, J. E. Spencer, D. Walz, S. C. Berridge, W. M. Bugg, K. Shmakov, A. W. Weidemann, C. Bula, K. T. McDonald, E. J. Prebys, C. Bamber, S. J. Boege, T. Koffas, T. Kotseroglou, A. C. Melissinos,

D. D. Meyerhofer, D. A. Reis, and W. Ragg, Phys. Rev. Lett. **79**, 1626 (1997).
[6] J. M. Cole, K. T. Behm, E. Gerstmayr, T. G. Blackburn, J. C. Wood, C. D. Baird, M. J. Duff, C. Harvey, A. Ilderton *et al.*, Phys. Rev. X **8**, 011020 (2018).
[7] K. Poder, M. Tamburini, G. Sarri, A. Di Piazza, S. Kuschel, C. D. Baird, K. Behm, S. Bohlen, J. M. Cole, D. J. Corvan *et al.*, Phys. Rev. X **8**, 031004 (2018).
[8] ELI-beamlines: https://www.eli-beams.eu/
[9] S. Gales, K. A. Tanaka, D. L. Balabanski, F. Negoita, D. Stutman, O. Tesileanu, C. A. Ur, D. Ursescu, I. Andrei, S. Ataman *et al.*, Rep. Prog. Phys. **81**, 094301 (2018).
[10] CoReLS: https://corels.ibs.re.kr
[11] B. Le Garrec, D. N. Papadopoulos, C. Le Blanc, J. P. Zou, G. Chériaux, P. Georges, F. Druon, L. Martin, L. Fréneaux, A. Beluze, N. Lebas, F. Mathieu, and P. Audebert, in *High-Power, High-Energy, and High-Intensity Laser Technologies III*, edited by J. Hein, SPIE Proc. Vol. No. 10238 (SPIE, Bellingham, 2017).
[12] XCELS: http://www.xcels.iapras.ru
[13] C. Hernandez-Gomez, S. P. Blake, O. Chekhlov, R. J. Clarke, A. M. Dunne, M. Galimberti, S. Hancock, R. Heathcote, P. Holligan, A. Lyachev, P. Matousek, I. O. Musgrave, D. Neely, P. A. Norreys, I. Ross, Y. Tang, T. B. Winstone, B. E. Wyborn, and J. Collier, J. Phys. Conf. Ser. **244**, 032006 (2010).
[14] Advanced accelerator development strategy report: Doe advanced accelerator concepts research roadmap workshop, U.S. DOE Office of Science Report No. 1358081, 2016 (unpublished).
[15] L. S. Brown and T. W. B. Kibble, Phys. Rev. **133**, A705 (1964).
[16] A. I. Nikishov and V. I. Ritus, Sov. Phys. JETP **19**, 529 (1964).
[17] I. Goldman, Phys. Lett. **8**, 103 (1964).
[18] G. Breit and J. A. Wheeler, Phys. Rev. **46**, 1087 (1934).
[19] H. R. Reiss, J. Math. Phys. **3**, 59 (1962).
[20] F. Sauter, Z. Phys. **69**, 742 (1931).
[21] W. Heisenberg and H. Euler, Z. Phys. **98**, 714 (1936).
[22] J. Schwinger, Phys. Rev. **82**, 664 (1951).
[23] A. R. Bell and J. G. Kirk, Phys. Rev. Lett. **101**, 200403 (2008).
[24] A. M. Fedotov, N. B. Narozhny, G. Mourou, and G. Korn, Phys. Rev. Lett. **105**, 080402 (2010).
[25] S. S. Bulanov, T. Z. Esirkepov, A. G. R. Thomas, J. K. Koga, and S. V. Bulanov, Phys. Rev. Lett. **105**, 220407 (2010).
[26] S. S. Bulanov, C. B. Schroeder, E. Esarey, and W. P. Leemans, Phys. Rev. A **87**, 062110 (2013).
[27] S. S. Bulanov, V. D. Mur, N. B. Narozhny, J. Nees, and V. S. Popov, Phys. Rev. Lett. **104**, 220404 (2010).
[28] I. Gonoskov, A. Aiello, S. Heugel, and G. Leuchs, Phys. Rev. A **86**, 053836 (2012).
[29] A. Gonoskov, I. Gonoskov, C. Harvey, A. Ilderton, A. Kim, M. Marklund, G. Mourou, and A. Sergeev, Phys. Rev. Lett. **111**, 060404 (2013).
[30] I. Bassett, Opt. Acta **33**, 279 (1986).
[31] E. G. Gelfer, A. A. Mironov, A. M. Fedotov, V. F. Bashmakov, E. N. Nerush, I. Y. Kostyukov, and N. B. Narozhny, Phys. Rev. A **92**, 022113 (2015).
[32] M. Vranic, T. Grismayer, R. A. Fonseca, and L. O. Silva, Plasma Phys. Control. Fusion **59**, 014040 (2016).
[33] A. Gonoskov, A. Bashinov, S. Bastrakov, E. Efimenko, A. Ilderton, A. Kim, M. Marklund, I. Meyerov, A. Muraviev, and A. Sergeev, Phys. Rev. X **7**, 041003 (2017).
[34] A. Gonoskov, A. Bashinov, I. Gonoskov, C. Harvey, A. Ilderton, A. Kim, M. Marklund, G. Mourou, and A. Sergeev, Phys. Rev. Lett. **113**, 014801 (2014).
[35] J. G. Kirk, Plasma Phys. Control. Fusion **58**, 085005 (2016).
[36] A. Gonoskov and M. Marklund, Phys. Plasmas **25**, 093109 (2018).
[37] S. V. Bulanov, T. Z. Esirkepov, J. Koga, and T. Tajima, Plasma Phys. Rep. **30**, 196 (2004).
[38] T. Z. Esirkepov and S. V. Bulanov, Phys. Lett. A **381**, 2559 (2017).
[39] A. M. Fedotov, N. V. Elkina, E. G. Gelfer, N. B. Narozhny, and H. Ruhl, Phys. Rev. A **90**, 053847 (2014).
[40] M. Jirka, O. Klimo, S. V. Bulanov, T. Z. Esirkepov, E. Gelfer, S. S. Bulanov, S. Weber, and G. Korn, Phys. Rev. E **93**, 023207 (2016).
[41] Z. Gong, R. H. Hu, Y. R. Shou, B. Qiao, C. E. Chen, X. T. He, S. S. Bulanov, T. Z. Esirkepov, S. V. Bulanov, and X. Q. Yan, Phys. Rev. E **95**, 013210 (2017).
[42] A. S. Samsonov, E. N. Nerush, and I. Y. Kostyukov, Phys. Rev. A **98**, 053858 (2018).
[43] S. V. Bulanov, T. Z. Esirkepov, J. K. Koga, S. S. Bulanov, Z. Gong, X. Q. Yan, and M. Kando, J. Plasma Phys. **83**, 905830202 (2017).
[44] T. Z. Esirkepov, S. S. Bulanov, J. K. Koga, M. Kando, K. Kondo, N. N. Rosanov, G. Korn, and S. V. Bulanov, Phys. Lett. A **379**, 2044 (2015).
[45] E. N. Nerush, I. Y. Kostyukov, A. M. Fedotov, N. B. Narozhny, N. V. Elkina, and H. Ruhl, Phys. Rev. Lett. **106**, 035001 (2011).
[46] R. Duclous, J. G. Kirk, and A. R. Bell, Plasma Phys. Control. Fusion **53**, 015009 (2011).
[47] I. V. Sokolov, N. M. Naumova, and J. A. Nees, Phys. Plasmas **18**, 093109 (2011).
[48] C. Ridgers, J. Kirk, R. Duclous, T. Blackburn, C. Brady, K. Bennett, T. Arber, and A. Bell, J. Comput. Phys. **260**, 273 (2014).
[49] A. Gonoskov, S. Bastrakov, E. Efimenko, A. Ilderton, M. Marklund, I. Meyerov, A. Muraviev, A. Sergeev, I. Surmin, and E. Wallin, Phys. Rev. E **92**, 023305 (2015).
[50] F. Niel, C. Riconda, F. Amiranoff, R. Duclous, and M. Grech, Phys. Rev. E **97**, 043209 (2018).
[51] J. Derouillat, A. Beck, F. Pérez, T. Vinci, M. Chiaramello, A. Grassi, M. Flé, G. Bouchard, I. Plotnikov, N. Aunai, J. Dargent, C. Riconda, and M. Grech, Comput. Phys. Commun. **222**, 351 (2018).
[52] E. S. Efimenko, A. V. Bashinov, S. I. Bastrakov, A. A. Gonoskov, A. A. Muraviev, I. B. Meyerov, A. V. Kim, and A. M. Sergeev, Sci. Rep. **8**, 2329 (2018).
[53] E. S. Efimenko, A. V. Bashinov, A. A. Gonoskov, S. I. Bastrakov, A. A. Muraviev, I. B. Meyerov, A. V. Kim, and A. M. Sergeev, Phys. Rev. E **99**, 031201 (2019).
[54] J. Magnusson, A. Gonoskov, M. Marklund, T. Z. Esirkepov, J. Koga, K. Kondo, M. Kando, S. Bulanov, G. Korn, and S. Bulanov, Phys. Rev. Lett. **122**, 254801 (2019).
[55] T. G. Blackburn, A. Ilderton, M. Marklund, and C. P. Ridgers, New J. Phys. **21**, 053040 (2019).
[56] V. Yakimenko, S. Meuren, F. Del Gaudio, C. Baumann, A. Fedotov, F. Fiuza, T. Grismayer, M. J. Hogan, A. Pukhov, L. O. Silva, and G. White, Phys. Rev. Lett. **122**, 190404 (2019).
[57] T. Podszus and A. Di Piazza, Phys. Rev. D **99**, 076004 (2019).

[58] A. Ilderton, Phys. Rev. D **99**, 085002 (2019).
[59] L. A. Vainshtein, *Electromagnetic Waves* (Radio i Svyaz', Moscow,1988) [in Russian].
[60] D. B. Owen, M. Abramowitz, and I. A. Stegun, Technometrics **7**, 78 (1965).
[61] L. D. Landau and E. M. Lifshitz, *The Classical Theory of Fields*, 3rd ed. (Pergamon, Oxford, 1971).
[62] S. V. Bulanov, T. Z. Esirkepov, M. Kando, J. K. Koga, and S. S. Bulanov, Phys. Rev. E **84**, 056605 (2011).
[63] A. J. Gonsalves, K. Nakamura, J. Daniels, C. Benedetti, C. Pieronek, T. C. H. de Raadt, S. Steinke, J. H. Bin, S. S. Bulanov, J. van Tilborg *et al.*, Phys. Rev. Lett. **122**, 084801 (2019).
[64] A. Gonoskov, arXiv:1607.03755.
[65] A. Mironov, N. Narozhny, and A. Fedotov, Phys. Lett. A **378**, 3254 (2014).
[66] S. Meuren, C. H. Keitel, and A. Di Piazza, Phys. Rev. D **93**, 085028 (2016).
[67] D. Seipt, T. Heinzl, M. Marklund, and S. S. Bulanov, Phys. Rev. Lett. **118**, 154803 (2017).
[68] J. K. Koga and T. Hayakawa, Phys. Rev. Lett. **118**, 204801 (2017).
[69] M. Tamburini, A. Di Piazza, and C. H. Keitel, Sci. Rep. **7**, 5694 (2017).
[70] A. Sampath and M. Tamburini, Phys. Plasmas **25**, 083104 (2018).